Bio-Design and Manufacturing (2024) 7:938–954
https://doi.org/10.1007/s42242-024-00305-2

RESEARCH ARTICLE

3D-bioprinted tri-layered cellulose/collagen-based drug-eluting fillers for the treatment of deep tunneling wounds

Mano Govindharaj[1] · Noura Al Hashimi[1] · Soja S. Soman[1] · Jiarui Zhou[1,2] · Safeeya AlAwadhi[1] · Sanjairaj Vijayavenkataraman[1,2]

Received: 6 July 2023 / Accepted: 18 June 2024 / Published online: 22 October 2024

Abstract

Tunneling wounds create passageways underneath the skin surface with varying sizes and shapes and can have twists and turns, making their treatment extremely difficult. Available wound care solutions only cater to superficial wounds, and untreated tunneling wounds pose major health concerns. This study aims to fulfill this challenge by fabricating tunnel wound fillers (TWFs) made of natural polymers that mimic the dermal extracellular matrix. In this study, cellulose microfibers (CMFs) derived from banana stem and fish skin-derived collagen were used to formulate bio-inks with varying CMF contents (25, 50, and 75 mg). Tri-layered (CMFs, primary and secondary collagen coatings), drug-eluting (Baneocin), and cell-laden (human mesenchymal stem cells) TWFs were three-dimensional (3D)-printed and extensively characterized. CMFs showed the most suitable rheological properties for 3D printing at 50 mg concentration. The Alamar Blue data showed significantly increased cell proliferation from Day 1 to Day 7, and scratch tests used to evaluate in vitro wound healing revealed that the best coverage of the wound area was achieved using CMFs in combination with collagen and alginate. Finally, the TWF showed promising capability and tunability in terms of wound shape and size upon testing on a chicken tissue model. The results demonstrate the tremendous potential of TWFs in treating deep tunneling wounds with unique advantages, such as patient-specific customization, good wound exudate absorption capability while releasing wound healing drugs, and the inclusion of stem cells for accelerated healing and tissue regeneration.

✉ Sanjairaj Vijayavenkataraman
vs89@nyu.edu

[1] The Vijay Lab, Division of Engineering, New York University Abu Dhabi, Abu Dhabi 129188, UAE

[2] Department of Mechanical and Aerospace Engineering, Tandon School of Engineering, New York University, Brooklyn, NY 11201, USA

Graphic abstract

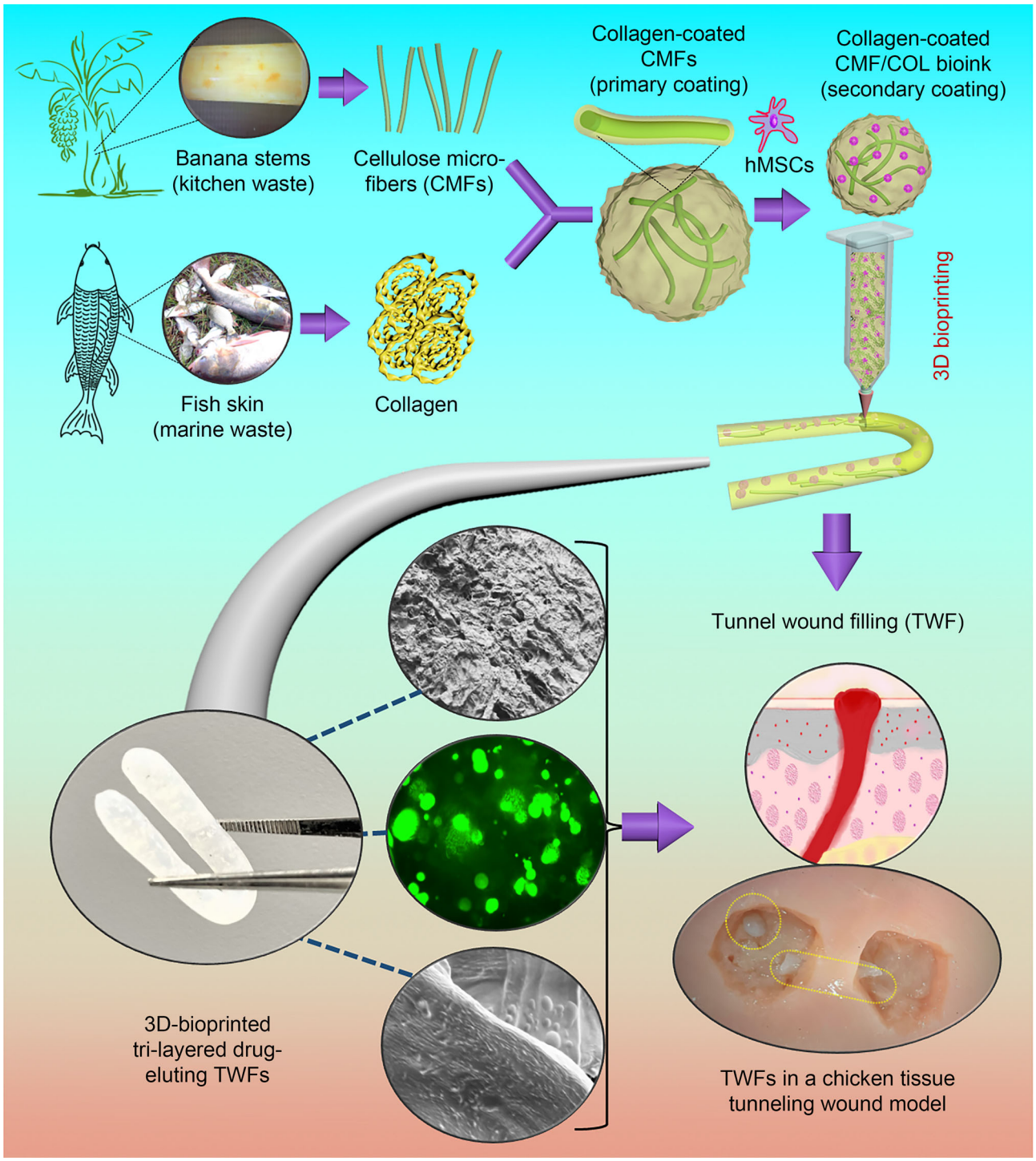

Keywords Bio-ink · Bioprinting · Cellulose · Fish collagen · 3D printing · Tunneling wounds

Introduction

The skin is the largest organ of a human body that protects the internal organs from external invasions [1]. Several complex and dynamic processes occur upon injuries, including inflammation, hemostasis, and maturation by cell proliferation [2]. Among them, tunneling wounds are particularly difficult to treat as they create passageways underneath the skin surface, which vary in depth and length and can take twists and turns. The tunnels can extend to form a full-thickness wound into and through the soft tissue of the subcutaneous muscle. The causes of tunneling wounds include infections associated with normal wounds, abscess formation, stalled healing, shear forces and pressure on the skin (e.g., pressure ulcers), comorbidities (e.g., diabetes), and prolonged drug use (e.g., antibiotics and corticosteroids) [3]. Available wound care solutions only cater to superficial or surface wounds, and the risk of untreated tunneling wounds poses major health concerns [4].

While there are no ideal treatment methods for tunneling wounds, several attempts have been made to use the acellular dermal matrix and biopolymer-based or hydrogel-based formulations in a sheet or paste form [5]. While the sheet form is a traditional wound dressing used for the treatment of superficial wounds that are rolled and packed into the tunneling wound, the paste form of the matrix or hydrogels is applied or packed directly into the wound, and the latter is preferred for ease of use [5]. Examples of sheet-based wound dressings include Graftjacket® regenerative tissue matrix [6] and AlloDerm® [7]. Although sheet-type wound dressings best suit superficial wounds, they are ineffective on tunneling wounds [5]. The limitations include the rolling of the sheet into required tunneling wound diameters and incomplete packing of the wound, which will result in stalled healing, secondary infections, and other complications. The use of paste-type matrices or hydrogels overcomes the limitations of sheet-type dressings and has been proven to be effective for treating shallow tunneling wounds, such as diabetic ulcers [8, 9]. However, paste-type matrices are not ideal for deep tunneling wounds. The disadvantages of paste-type matrix or hydrogels are felt during regular wound dressings as the cleaning of the tunnels becomes extremely difficult, and frequent dressings (to clean and pack the tunnels to prevent further infection) might expose the wound and the surrounding tissue to shear stresses and pressure, worsening the tunneling wounds. One solution is the use of bioprosthetic plugs, such as Gore Bio-A® Fistula Plug [10], but they show limitations, such as lack of biodegradation or long biodegradation time, the dehydration of the wound site, and high failure rates [11]. Recent studies have demonstrated the use of shape memory polymer hydrogels based on polyvinyl alcohol, cornstarch (CS) and gelipin for the treatment of Crohn's disease and other deep chronic wounds [11–14], as well as microspheres [15]. However, these materials are not ideal for tunneling wounds and cannot incorporate cells to accelerate the healing process in tertiary wounds.

In this work, a bioprinted tri-layered cellulose/collagen-based drug-eluting filler, referred to as the tunnel wound filler (TWF), is proposed as a potential treatment option for deep tunneling wounds to overcome the challenges of deep tunneling wound treatment and the limitations of available solutions. The role of collagen in wound healing is well-established owing to its bacterial resistance and biodegradability [16–18]. In particular, marine collagen derived from fish offers good biocompatibility for cell growth and mimics the native skin environment [19]. Furthermore, cellulose and cellulose fibers have been investigated as a potential wound dressing material [20], with the inclusion of antibacterial silver [21] or other growth factors [22]. The inclusion of cellulose fibers (micro/nano) contributes to the enhancement of mechanical properties [23]. Hence, fish collagen (COL) and cellulose microfibers (CMFs) were chosen as the two main components of the TWF. Extrusion-based three-dimensional (3D) bioprinting was used to fabricate the TWF to provide accurate constructs, which can be wound- and patient-specific with complex, chronic wound shapes. Sodium alginate (SA) was used to suspend collagen-coated CMFs, mainly for the post-printing crosslinking process, which would impart structural stability to the printed TWF constructs.

The proposed TWF, which involves bioprinted tri-layered cellulose/collagen-based drug-eluting fillers, offers many advantages compared to the current standard of care for tunneling wounds: (1) patient- and wound-specific customization based on the size of the wound, drug dosage depending on the healing rate, and the possibility to incorporate patient-derived cells; (2) CMF/collagen bioactive material-based structure that mimics the natural extracellular matrix and provides ease of insertion/removal while being structurally stable; (3) smooth outer surface and softness, thereby reducing the pressure on the wound and the surrounding tissues and preventing further tissue damage during insertion, removal, and physiological movements; (4) good wound exudate absorption capability while releasing wound healing drugs (the dosage of which can be controlled and modified with delayed healing). The tri-layer CMF/COL combination offers unique qualities as the collagen plays a biological role by allowing the TWF to closely mimic the native skin matrix, whereas cellulose provides mechanical strength and stability to the TWF; thus, it forms the main core of the construct, whereas collagen forms the outer layers. The third collagen layer is included after crosslinking with alginate to further enhance the biological compatibility. This tri-layer structure allows for more control and easier customization, allowing a myriad of drug combinations and release rates at different dosages. In addition, the sources

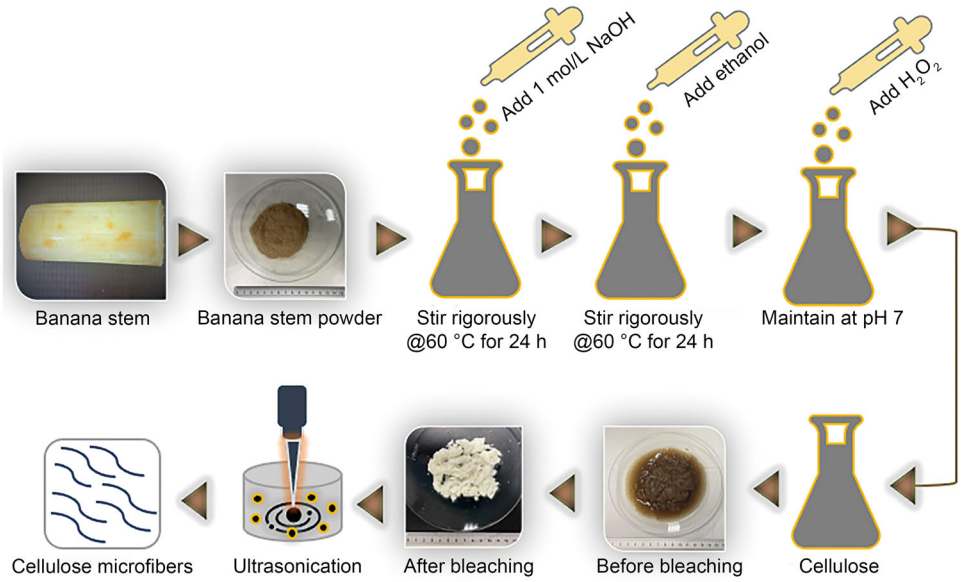

Fig. 1 Scheme depicting the chemical and mechanical procedures used to isolate cellulose microfibers (CMFs) from banana stems

of the biomaterials used in this work are environmentally friendly and sustainable. Collagen is derived from fish skin that was discarded, while CMFs are isolated from banana stems (kitchen waste), both contributing to a circular economy model.

This work can be divided into four parts: (1) sustainable utilization and extraction of CMFs from banana stems; (2) encapsulating CMFs in fish skin-derived collagen and the formulation and physicochemical characterization of the bioactive hydrogel; (3) bio-ink formulation, drug encapsulation, 3D printing and bioprinting of TWFs; (4) application of biologically active and structurally stable TWFs for tunnel wound care. After the thorough characterization of the microstructural, physiochemical, and mechanical properties, swelling rate, weight loss, and drug release rate, the biocompatibility of the 3D-bioprinted TWFs was evaluated using Alamar Blue (AB) metabolic activity and live/dead assay with human mesenchymal stem cells (hMSCs), and in vitro wound healing evaluation was performed using scratch tests with mouse embryonic fibroblasts (MEFs). Finally, the 3D-printed TWFs were tested for their suitability and applicability using the chicken tissue wound model for tunneling wound care applications.

Materials and methods

Isolation of CMFs

Figure 1 shows the procedure used to isolate CMFs from banana stems. Briefly, banana stems were collected from kitchen waste, dried at 40 °C in a hot air oven for three days, followed by air-drying, and powdered using a kitchen mixer grinder. Powdered fibers (100 mg) were soaked in 1 mol/L NaOH solution with rigorous stirring for 24 h at 60 °C. Consequently, the fibers were washed with Millipore water until the pH reached 7. The solution was filtered, washed, and lyophilized.

Bleaching and hydrolysis of cellulose

The lyophilized powder was dissolved in 500 mL of H_2O_2 solution at a ratio of 1:1 at 75 °C for 30-min bleaching. The sample was filtered and washed again with Millipore water. After bleaching, the banana stem-derived cellulose fibers were treated with 1% (volume fraction) H_2SO_4 for 1 h at 80 °C. After washing with water, the fibers were filtered and stored at 4 °C for the production of CMFs.

Ultrasonication

Ultrasonication using an ultrasonic probe at a specific amplitude of 70% for 4 h was performed to produce microfibers. To avoid overheating during sonication, the flask containing the fibers was placed in an ice bath. After sonication, the CMFs were separated using centrifugation at 4000 r/min for 30 min. The fibers were collected as pellets and stored at 4 °C for further studies.

Encapsulation of CMFs with fish skin-derived collagen

The discarded marine grouper fish skin waste bought from Zayed Port, Abu Dhabi, UAE, was sustainably utilized for collagen extraction according to a previously published procedure [24]. Collagen (200 mg) was diluted in 5 mL of

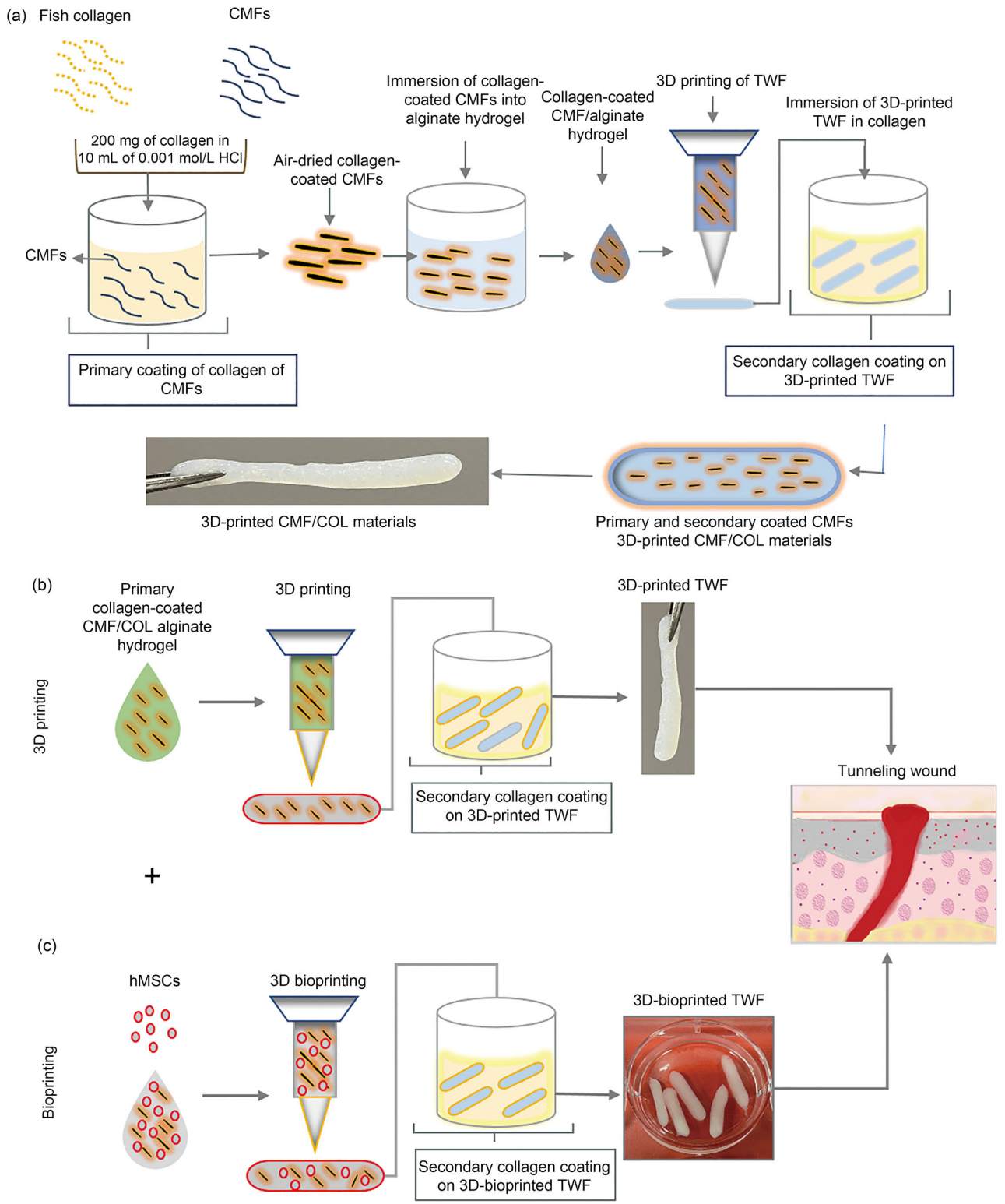

Fig. 2 **a** Scheme depicting the primary coating on CMFs and the secondary coating after the 3D printing of collagen-coated CMFs. **b** Scheme depicting the fabrication of 3D-printed TWFs. **c** 3D bioprinting of 50CMF/COL-based TWFs with hMSCs (200,000 cells per construct). CMFs: cellulose microfibers; hMSCs: human mesenchymal stem cells; TWFs: tunnel wound fillers; COL: collagen

phosphate-buffered saline (PBS) while maintaining the pH value at 7.4 using a magnetic stirrer and then neutralized. PBS was chosen owing to its similarity to physiological conditions in pH and ionic composition [25]. The solution was incubated for 2 h at 37 °C for hydrogel formation. CMFs in various ratios (25, 50, and 75 mg by weight) were prepared, named 25CMFs, 50CMFs, and 75CMFs, respectively, based on the CMF content. CMFs were mixed with the collagen solution and stirred overnight for complete encapsulation. Afterward, the hydrogels were lyophilized and stored at 4 °C for hydrogel formulation. The procedure is illustrated in Fig. 2a.

Characterization of CMF/COL hydrogels

The lyophilized CMF/COL fibers were imaged using scanning electron microscopy (SEM, Quanta^{TM} 450 FEG, FEI Company, USA). Fourier transform infrared (FTIR) spectroscopy (Invenio S, Bruker, USA) was used for the analysis of the functional groups of CMF/COL hydrogels in the range of 400–4000 cm^{-1}. A thermogravimetric analyzer (TGA, TG209 F1 Libra, Netzsch, Germany) was used to evaluate the thermal stability of CMF/COL fibers. To check the crystalline structure of CMFs, X-ray diffraction (XRD, Empyrean 3, Malvern Panalytical Pvt. Ltd., UK) was used at room temperature from 2° to 400° (2θ). To confirm collagen coating on CMF fibers, Raman spectroscopy (alpha 300, WITec, Germany) was used and Raman spectra were recorded in the range of 0–3500 cm^{-1} using a 600-mW laser. The mechanical and compressive properties of 3D-printed TWFs were measured using the MACH-1 v500 (Biomomentum Inc., Canada) instrument.

3D printing of TWFs

Rheology tests

SA was used for suspending collagen-coated CMFs, mainly for the post-printing crosslinking process that would impart structural stability to the printed TWF constructs. SA (25 mg; Spectrum® Chemical Mfg. Corp., Gardena, CA, USA) was added to the three CMF/COL lyophilized powders in 4 mL of Dulbecco's modified Eagle's medium (DMEM) and stirred thoroughly to develop a 3D printable ink. ElastoSens Bio 2 (Rheolution Inc., Canada) was used to characterize the rheological properties at different concentrations of CMF hydrogels. A minimum hydrogel volume of 4 mL was required for each test and one test lasted 90 min to reach a steady state. All the tests were performed at 24 °C (room temperature). Shear storage modulus and shear loss modulus over time were obtained.

3D printing of TWF hydrogels

The RegenHU 3D-Discovery bioprinter (RegenHU Ltd., Switzerland) was used for the 3D printing of TWFs (Fig. 2b). The formulated ink (3 mL) was filled into the cartridge and printed using a conical needle with an internal diameter of 1.5 mm, a feed rate of 4 mm/s, and a pressure of 0.03 MPa. After successful printing, the construct was ionically crosslinked with 250 mmol/L $CaCl_2$ for 5 min to obtain a stable structure and washed gently with PBS. In the bioprinted constructs (Fig. 2c), the same formulation was used with 200,000 cells per construct. Consequently, they were used for subsequent characterizations and experiments.

Swelling/degradation test

To analyze the swelling ratio (SR), lyophilized TWFs were weighed (W_i) and soaked in PBS solution at room temperature. At specified time points (1, 6, 12, 24, 48, and 72 h), the sample was taken out and weighed (W_t). The SR is described by the following equation:

$$\mathrm{SR} = \frac{W_t - W_i}{W_i} \times 100\%. \tag{1}$$

Similarly, degradation rate (DR) experiments were conducted with specific modifications. The TWF sample was soaked in PBS, taken out at the defined time points, lyophilized, and then weighed (W_{dt}). The DR is described by the following equation:

$$\mathrm{DR} = \frac{W_i - W_{dt}}{W_i} \times 100\%. \tag{2}$$

In vitro release rate of Baneocin

An in vitro drug release study was performed to analyze the drug release rate of TWFs coated with Baneocin powder (a common skin antibiotic drug) at different pH values. Baneocin-coated TWFs were immersed in 1 mL of the simulated body fluid (pH 7.4, PBS) or diluted HCl (pH 5) and gently rotated at 100 r/min. At predetermined intervals (0, 2, 6, 12, 24, and 48 h), 200 μL of the solution was taken out, while the same volume of the fresh solution was replaced accordingly to maintain the original volume of 1 mL. The amount of Baneocin released was determined by measuring the absorbance at 310 nm. All experiments were performed in triplicate.

Biocompatibility evaluation of 3D-bioprinted TWFs

Cell culture

Commercially acquired human mesenchymal stem cells (hMSCs) (immortalized human bone marrow mesenchymal stromal cells, hTERT iMSC3, Catalog No. T0529, Applied Biological Materials Inc., Richmond, BC, Canada) were cultured in DMEM media (DMEM supplemented with 2 mmol/L L-glutamine, 5% fetal bovine serum (FBS), and 1% penicillin–streptomycin). The culture was further maintained in an incubator (5% CO_2, 37 °C) for proliferation. Cells were trypsinized, sub-cultured, and harvested for 3D bioprinting after confluency. All the bio-ink preparation was conducted under sterile cell culture conditions in a laminar airflow chamber. The 3D bioprinting hood was properly sterilized using 70% ethanol and ultraviolet (UV) for 4 h before printing. Each 3D CMF/COL-based TWF construct was bioprinted with 200,000 cells for all the subsequent biological experiments.

Bio-ink preparation and bioprinting

The bio-ink preparation was conducted using the procedure described in our previous article [26]. Figure 2c shows the schematic representation of the 3D bioprinting process. In detail, the 50CMF/COL bio-ink was mixed with 25 mg of SA (Spectrum® Chemical Mfg. Corp., Gardena, CA, USA) in 4 mL of DMEM media to develop a 3D printable ink; hMSCs were then mixed (200,000 cells/construct) and loaded into a 3-mL extrusion cartridge, and bioprinting was performed using a needle with an internal diameter of 1.5 mm at a feed rate of 4 mm/s and a pressure of 0.03 MPa. After successful bioprinting, the TWF constructs were ionically crosslinked with 250 mmol/L $CaCl_2$ for 5 min, followed by 15 min of incubation in 0.2% FBS solution. Then, the bioprinted constructs were immediately transferred to cell culture media (DMEM with 10% FBS and 1% penicillin–streptomycin) and incubated at standard culture conditions.

Cell viability and proliferation

To quantitatively analyze the cell proliferation of hMSCs in 3D-bioprinted TWF constructs, the AB assay (BioSource International, Camarillo, CA, USA) was used to measure the metabolic activity as per the manufacturer's protocol. Live/dead staining with calcein AM and ethidium homodimer-1 (LIVE/DEAD™ Viability/Cytotoxicity Kit, Thermo Fisher Scientific, USA) was performed to visualize the viability of hMSCs in the 3D constructs as per the manufacturer's protocol. Imaging was performed using a Leica SP8 confocal laser scanning microscope.

In vitro wound healing assay

In vitro cell migration studies with MEF cells were performed to evaluate the wound healing potential using a previously described method [27]. Briefly, 200,000 cells/mL were seeded in 6-well plates and cultured overnight. Consequently, the cells were washed with PBS, and a scratch of 1 mm width was gently created using a sterile pipette tip. PBS was used to remove the detached cells with gentle washing. Cells were treated with 100 μL of the collagen solution and Baneocin (a standard drug used in wound healing) extract and incubated for 24 h. Untreated cells were used as the negative control. Images were taken using an inverted microscope. ImageJ wound healing size tool plugin was used to measure the change in the wound area over 24 and 48 h. The line graph was normalized to the initial area for each condition. All experiments were performed in triplicate ($n = 3$).

Chicken tissue model for tunneling wounds

To check the suitability and applicability of 3D-printed TWFs, a chicken breast tissue wound model was developed. Briefly, a whole chicken tissue was purchased from the market, and two full-thickness wounds were created on the side of the breast with deep tunneling (depth: 1.5 cm) using a surgical knife. Then, 3D-printed TWFs were inserted into the deep tunneling wounds to evaluate their applicability.

Statistical analysis

All experiments were conducted with $n = 3$, and the numerical and graph results are illustrated as mean ± standard deviation (SD). Data significance was determined using a two-tailed t test per group where $P < 0.05$ is considered significant.

Results

Extraction, formulation, and characterization of CMF/COL inks

After the step-by-step isolation process as described in Sect. "Materials and methods," CMFs were coated with fish skin-derived collagen (COL) (Figs. 3a–3c) to improve their bioactivity. The representative images of 50CMF/COL are shown in Figs. 3a–3c, and the same procedure was followed for the other two concentrations (the primary collagen coating).

The difference between the surfaces coated with collagen and those without collagen can be clearly seen in the SEM images shown in Figs. 3g–3l. CMFs without the primary collagen coating have a smooth surface (Figs. 3g–3i),

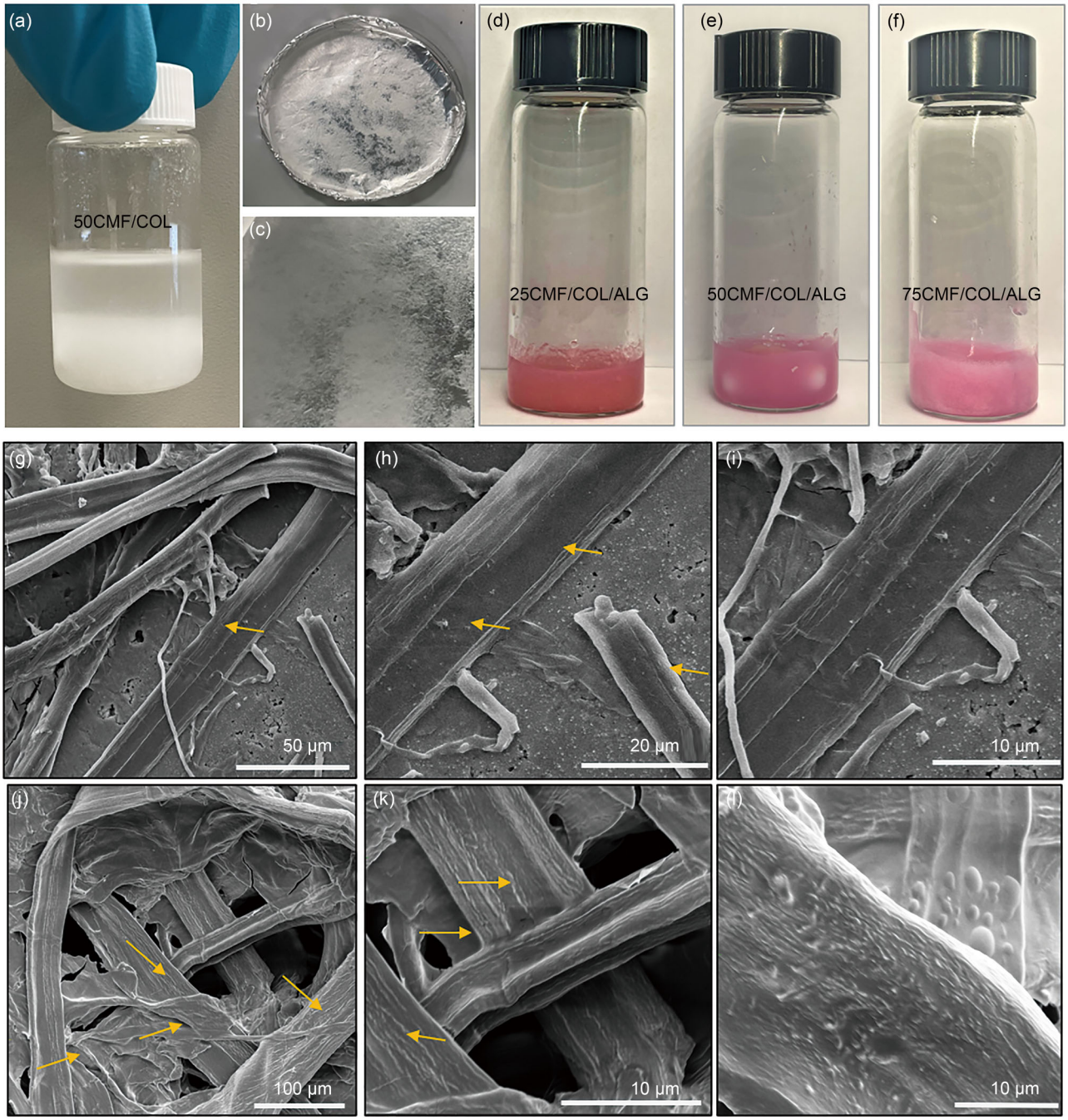

Fig. 3 **a–f** Formulation of CMF/COL and CMF/COL/ALG for the fabrication of TWFs: **a** process of collagen coating on CMFs; **b**, **c** air-drying of collagen-coated CMFs; **d–f** three different concentrations of CMF/COL/ALG hydrogels. **g–l** SEM micrographs of CMFs without the primary collagen coating (**g–i**) and with the primary collagen coating (**j–l**). CMFs: cellulose microfibers; TWFs: tunnel wound fillers; SEM: scanning electron microscopy; COL: collagen; ALG: alginate

whereas CMFs coated with collagen have a rough and wavy surface (Figs. 3j–3l). It can also be seen from Figs. 3j–3l that the CMFs are completely covered with collagen, proving the effectiveness of the coating.

To support the observations made using SEM, CMFs, collagen, and the CMF/COL ink were characterized by FTIR spectroscopy to determine the presence of collagen over CMFs. The FTIR spectra of CMFs, COL (collagen), and the 50CMF/COL ink are shown in Fig. 4a. The peaks obtained at approximately 3289, 2926, 1634, and 1535 cm^{-1} for the 50CMF/COL ink correspond to the O–H & N–H, C = O, and amide stretching vibrations, respectively. These are the main

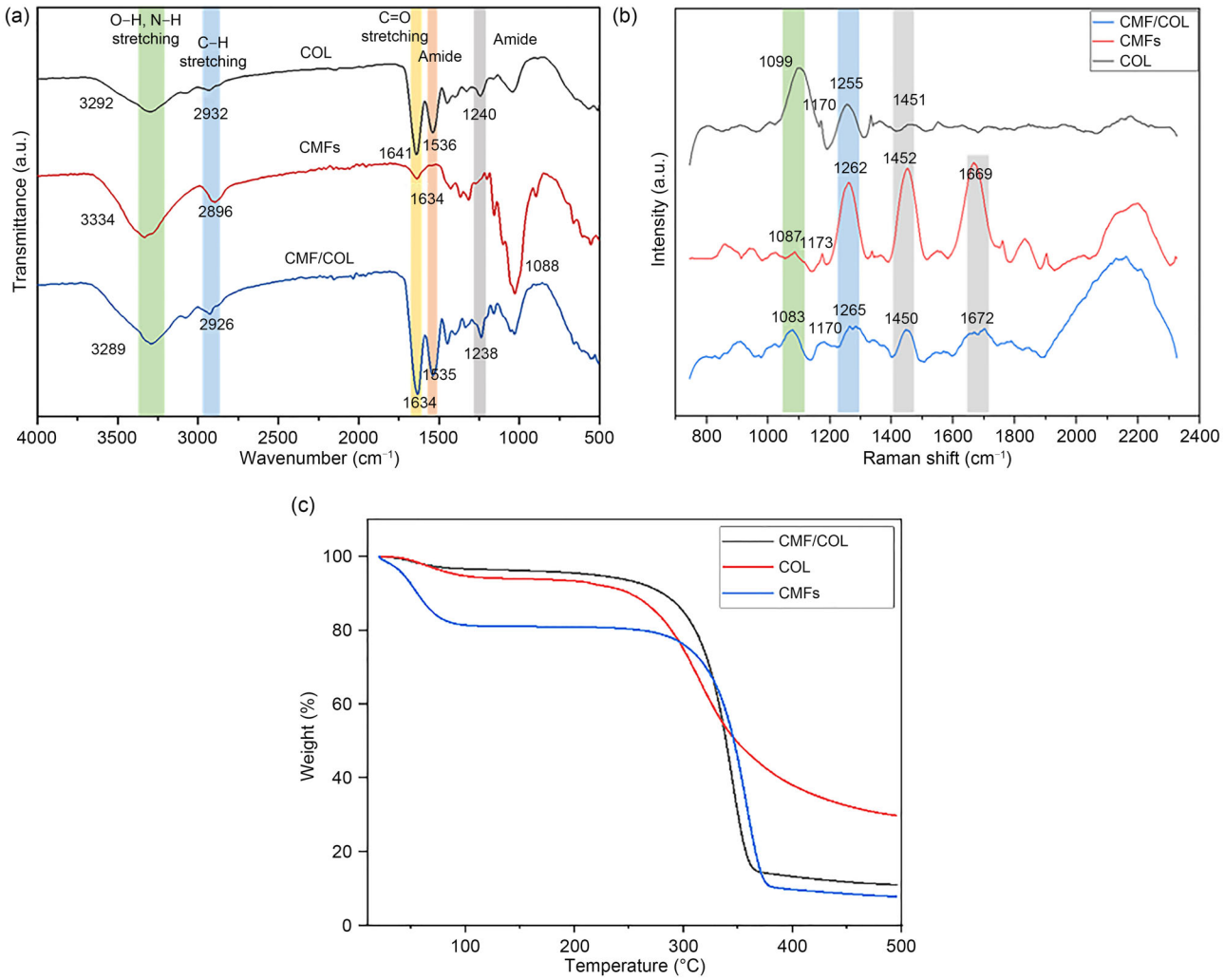

Fig. 4 **a** FTIR spectra of CMFs, COL, and the CMF/COL hydrogels. **b** Raman spectra of CMFs, COL, and the CMF/COL hydrogels. **c** TGA thermogram of CMFs, COL, and the CMF/COL hydrogels. FTIR: Fourier transform infrared; CMFs: cellulose microfibers; COL: collagen; TGA: thermogravimetric analyzer

functional groups for CMFs and collagen, which were also present in pure CMFs and pure collagen. In the CMF/COL ink, the bands corresponding to N–H and O–H stretching shifted to the lower wavenumber of 3289 cm^{-1} (3334 cm^{-1} for CMFs), while the C = O bands of CMF/COL shifted to 1634 cm^{-1}. Some shifts in the characteristic peaks of CMFs and collagen were observed in the CMF/COL ink. The broad peaks at 3289 cm^{-1} corresponding to the N–H stretching vibrations of the amine groups of fish-derived collagen could interact with the O–H stretching of CMFs [28, 29].

Further, the successful coating of CMFs with collagen was confirmed using Raman spectroscopic analysis (Fig. 4b), indicating the presence of cellulose and collagen in the CMF/COL formulation. The spectral data of lyophilized CMFs, collagen, and the CMF/COL material showed peaks at 1170, 1265, and 1672 cm^{-1}, indicating the presence of collagen [30]. The characteristic peaks representing cellulose at 1083 and 1450 cm^{-1} were also observed [31]. The main characteristic peaks for CMFs and collagen were present in the CMF/COL ink. These results confirm the successful coating of collagen on the CMFs.

Figure 4c shows the TGA thermograms of CMFs, COL, and the CMF/COL ink. For collagen, the major weight loss occurred in the range of 200–500 °C, and for CMFs, it occurred between 300 and 400 °C (indicating the decomposition of cellulose). In both collagen and CMFs, the first thermal degradation mainly indicates the loss of free and bound water molecules [31]. The data show that the thermal stability of the CMF/COL composite was improved compared to pure collagen owing to the crosslinking and association of cellulose and collagen molecules [32]. While

the onset temperature of pure collagen was in the range of 150–250 °C, the thermal degradation range of both CMFs and CMF/COL was 300–400 °C, with more than 70% weight loss happening within this range.

Rheology, 3D printing, and secondary collagen coating of CMF/COL/ALG inks

Three different concentrations of CMF/COL/ALG inks (25CMF/COL/ALG, 50CMF/COL/ALG, and 75CMF/COL/ALG) were prepared, as shown in Figs. 3d–3f. The printability of the three ink formulations was evaluated, as shown in Figs. 5a–5c. While the 25CMF/COL/ALG ink completely covered the pores, the 50CMF/COL/ALG and 75CMF/COL/ALG inks had better printability. The viscosity of the inks increased with increasing CMF concentration, with 25CMF/COL/ALG having the lowest viscosity and 75CMF/COL/ALG having the highest viscosity. This can also be explained by the rheological properties of these inks, shown in Fig. 5d. All the inks had a higher storage modulus than loss modulus, indicating that the ink behaves more like a gel than a solution and that the magnitude of the modulus increases with increasing CMF concentration.

Figure 5e shows the SR of the three different CMF/COL/ALG-based TWF constructs. The SR increased exponentially for 6 h (around 250%–300% from the initial dry weight) after which the fluid uptake stabilized at an equilibrium state. The presence of hydrophilic groups in the CMFs contributes to these high SRs [33]. This is proven by the data (Fig. 5e), where the increased concentration of CMFs led to a higher swelling ratio. For example, after 12 h, the swelling ratios of the 25CMF/COL/ALG, 50CMF/COL/ALG, and 75CMF/COL/ALG inks were (294 ± 14)%, (316 ± 21)%, and (348 ± 15)%, respectively.

Figure 5f shows the weight loss profiles of TWF constructs monitored for 72 h. A controlled weight loss over time was observed in all three groups. The degradation in weight is contributed by two factors: the release of collagen and the breaking of crosslinked polymeric chains. The rate of degradation mostly follows the CMF concentration, and the DR decreases as the CMF concentration increases.

Figure 5g shows the 3D-printed TWF using the 50CMF/COL/ALG ink immediately after printing and crosslinking. Once the constructs were printed, the secondary collagen coating was performed over the printed TWF constructs (tubular constructs are shown in Fig. 5g). The SEM images of the printed constructs with and without secondary collagen are shown in Fig. 6. Similar to the observations after the primary collagen coating, the surfaces without the secondary collagen coating (Figs. 6a–6c) were smooth compared to those with the secondary collagen coating (Figs. 6d–6f).

Drug-loaded TWFs

The prospects of drug-loaded TWFs for wound healing were evaluated with Baneocin. Baneocin is a widely used antibiotic for treating skin infections, and it was found to be an effective antibacterial drug. In this study, two sets of TWFs were used. The first set of TWFs was the same as that fabricated previously, as shown in Fig. 5g, with the secondary collagen coating on 3D-printed TWFs (50CMF/COL/ALG). The second set comprised 3D-printed TWFs (50CMF/COL/ALG) coated with Baneocin solution instead of the secondary collagen coating, with all the other procedures and parameters being the same. Different pH values were selected to mimic different environments, such as pH 5 to mimic a slightly acidic infectious state and pH 7 for the neutral state [34]. Figure 7 shows that the cumulative release profile of Baneocin normalized to the collagen only controls at acidic and neutral pH. All the release profiles showed an increasing release with time as expected, with a higher release rate and burst release at pH 5.

Fabrication, 3D printing, and bioprinting of TWFs

After successfully proving that drug-loaded TWFs can be fabricated, we attempted to incorporate stem cells into the 50CMF/COL/ALG ink to bioprint cell-laden TWFs. hMSCs were used in this study. Figure 8j shows the bioprinted hMSC-laden TWFs. The bio-ink supported the survival, growth, and proliferation of cells, as shown in Fig. 8. The live/dead staining and 4',6-diamidino-2-phenylindole (DAPI) staining images of hMSCs on Day 3 are shown in Figs. 8b and 8c respectively, whereas Fig. 8a shows the control with no cell for Day 3. Similarly, the live/dead staining and DAPI staining images of hMSCs on Day 5 are shown in Figs. 8e and 8f respectively (Fig. 8d shows the control with no cell for Day 5) and the images on Day 7 are shown in Figs. 8h and 8i respectively (Fig. 8g shows the control with no cell for Day 7). Cell viability was also quantitatively measured using the AB assay, and the results shown in Fig. 8k corroborate the qualitative live/dead and DAPI staining results. There is significant cell proliferation on Day 7 compared to that on Day 1, as shown in Fig. 8k.

Scratch test for the evaluation of in vitro wound healing

To evaluate the wound healing potential, 100 μL of the pure alginate (ALG), CMF/ALG, and CMF/COL/ALG extracts was added to each well containing MEFs. The results are shown in Fig. 9. Figures 9a–9d show the images taken immediately after scraping the cell layer, which formed a breach, and the migratory potential of MEFs is shown in

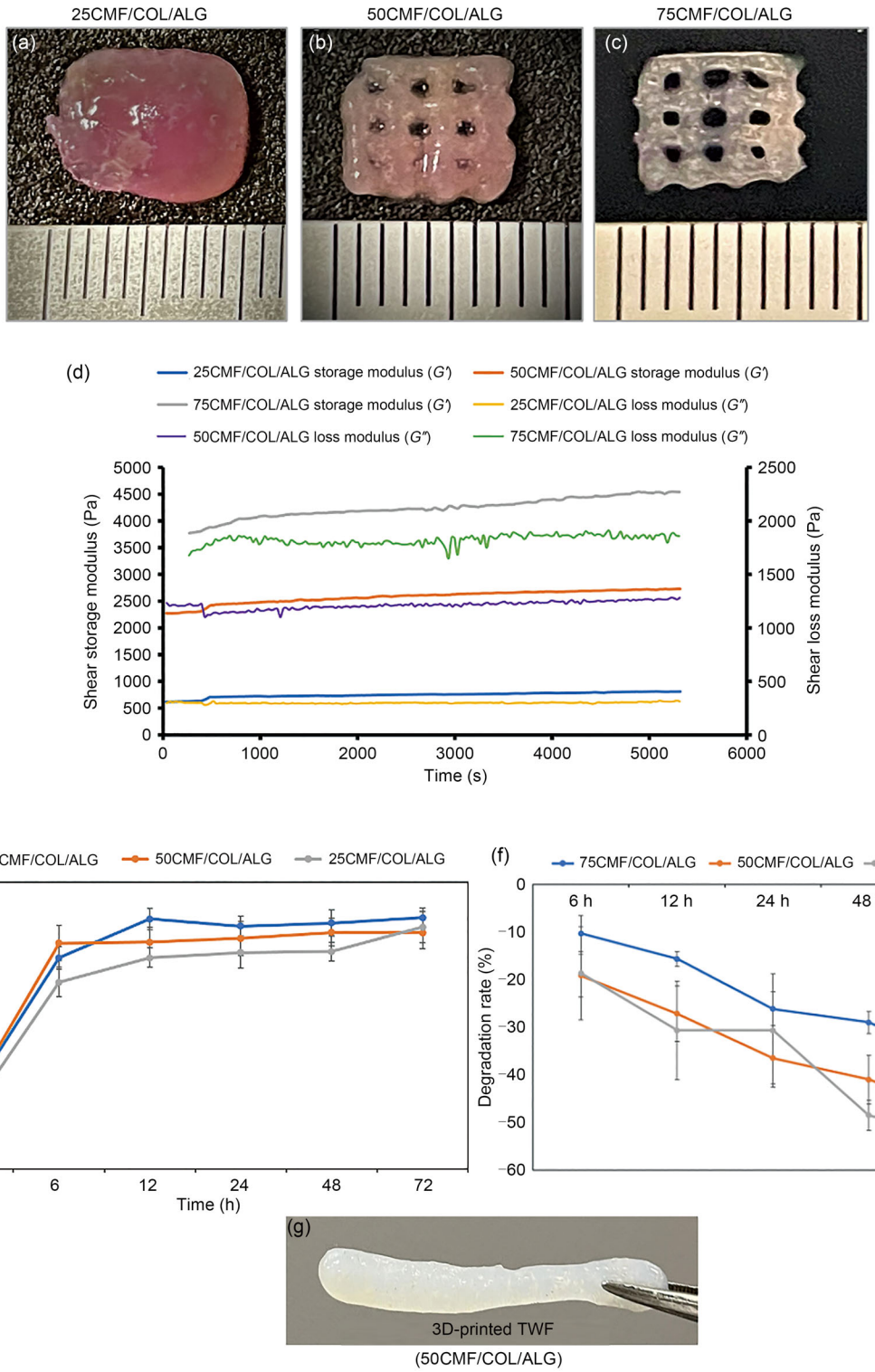

Fig. 5 3D printability of **a** 25CMF/COL/ALG, **b** 50CMF/COL/ALG, and **c** 75CMF/COL/ALG hydrogels, and **d** rheological properties, **e** swelling ratio, and **f** degradation rate of **g** 3D-printed TWF with the 50CMF/COL/ALG ink immediately after crosslinking. Data in (**e**, **f**) are expressed as mean±SD (n=3). CMFs: cellulose microfibers; COL: collagen; ALG: alginate; SD: standard deviation

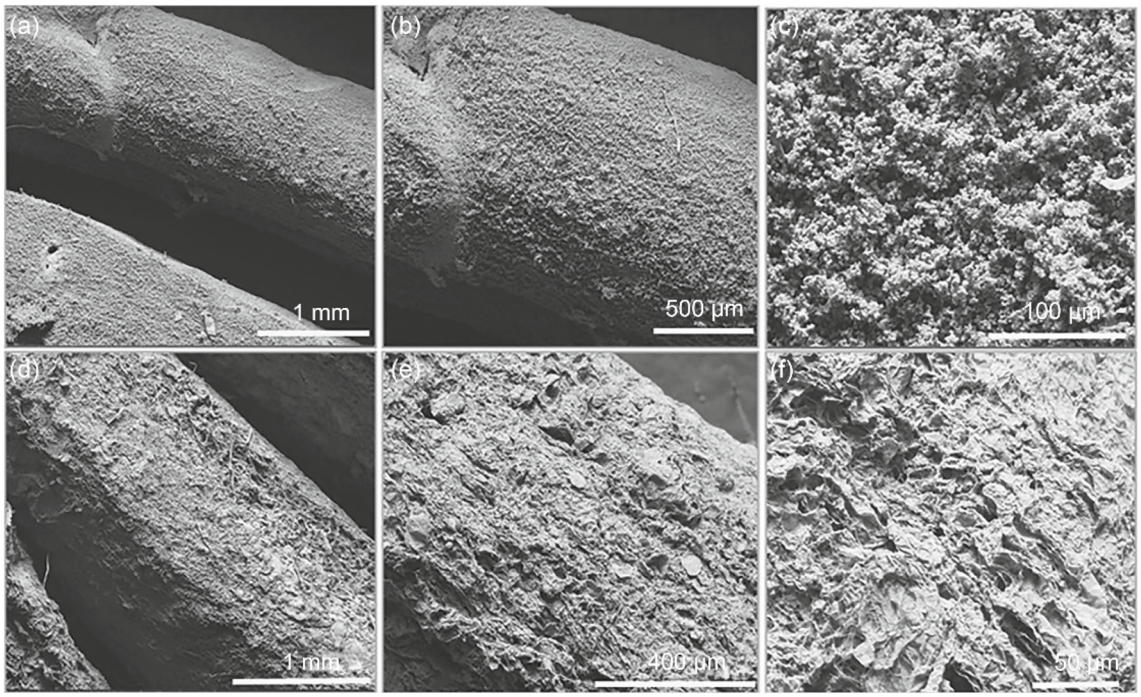

Fig. 6 SEM micrographs of cellulose-based 3D-printed TWFs with and without secondary collagen coating: **a**–**c** smooth surfaces of TWFs without collagen coating; **d**–**f** rough surfaces of TWFs indicating the post-printing collagen coating. SEM: scanning electron microscopy; TWFs: tunnel wound fillers

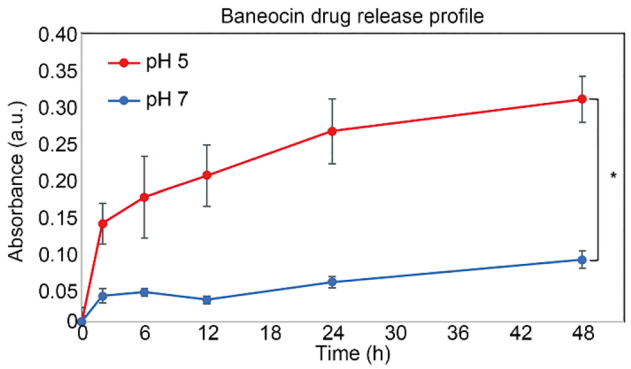

Fig. 7 Drug (Baneocin) cumulative release profile in acidic and neutral environments over 48 h. Data are expressed as mean ± SD ($n = 3$, $^{*}p \leq 0.05$). SD: standard deviation

Figs. 9e–9h (24 h) and Figs. 9i–9l (48 h). Figure 9m provides the quantified scatter plot data, showing that while MEFs migrated well in the presence of all hydrogels, those treated with CMF/COL/ALG almost completely covered the scratched wound areas in 48 h. The other two groups ALG and CMF/ALG, although performed better than the control group, did not completely cover the wound areas.

Testing of 3D-printed TWFs on the chicken tissue wound model

A chicken tissue model was used to demonstrate the suitability of using 3D-printed TWFs for tunneling wound care applications. Two deep tunnel wounds with a diameter of 5 mm and a length of 1.5 cm were formed on the chicken tissue as described in Sect. "Materials and methods," and the 3D-printed TWFs were inserted into the wounds.

Figures 10a and 10b show the 3D-printed TWFs inserted into the wounds. As shown in Fig. 10a, the structural stability and flexibility of the 3D-printed 50CMF/COL/ALG TWF indicated that the TWF hydrogel is suitable for insertion into deep tunneling wounds with twists and turns. The 3D-printed TWF revealed a smooth surface and softly curved edges with a moist environment (Fig. 10b). After creating two deep tunneling wounds (Fig. 10c), each wound was filled with the 3D-printed TWFs (Fig. 10d). Video S1 (Supplementary Information) demonstrated the creation of tunneling wounds and the insertion of the TWFs.

Discussion

Tunneling wounds are among the most difficult skin injuries to treat as they can create deep and complex wounds under the

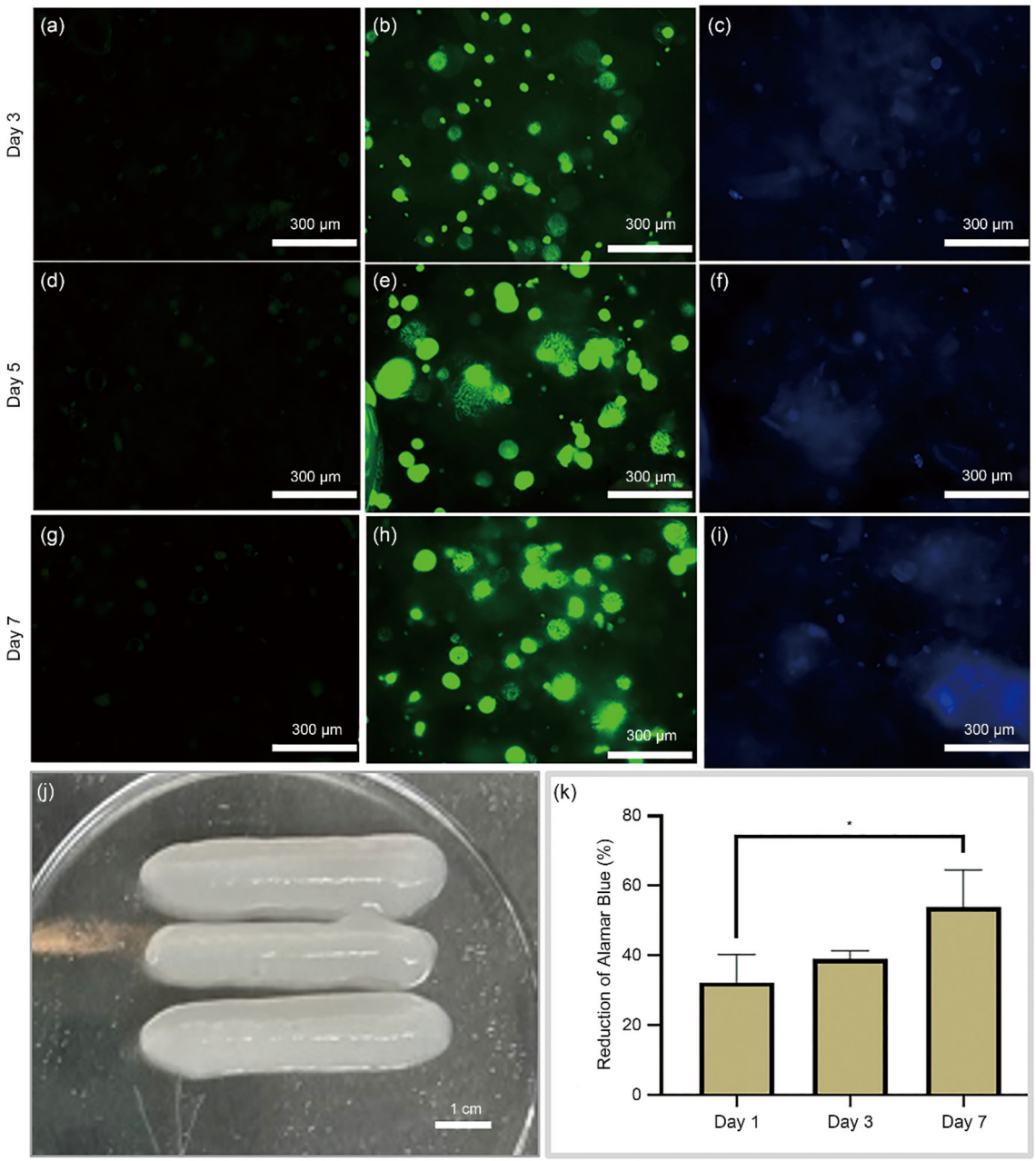

Fig. 8 Live/dead staining of hMSCs in 3D-bioprinted TWF tissue constructs on Days 3, 5, and 7 (green: viable cells). **a**, **d**, **g** control groups without cells. **b**, **e**, **h** Fluorescent staining of cells counterstained using calcein AM and ethidium homodimer-1. **c**, **f**, **i** Fluorescent staining of cell nuclei in bioprinted TWF tissue constructs counterstained using DAPI. **j** 3D-bioprinted TWF constructs. **k** AB assay bar graph on Days 1, 3, and 7 for cell proliferation. Data are expressed as mean ± SD ($n = 3$, $^{*}p \leq 0.05$). hMSCs: human mesenchymal stem cells; AB: Alamar Blue; AM: acetoxymethyl ester form; DAPI: 4',6-diamidino-2-phenylindole; TWFs: tunnel wound fillers

skin surface [3]. Available solutions only cater to superficial wounds; however, several new treatment options have been researched such as biopolymer sheets or pastes [5], acellular alternatives [8, 9], and shape memory polymers [13]. The aforementioned methods have limitations regarding proper wound packing, accessing the deep wound area, compatibility, and biodegradability.

In this work, we proposed a tri-layered cellulose/collagen-based drug-eluting filler (TWF) to overcome these challenges. Initially, the CMFs were successfully coated with collagen as the primary coating to enhance bioactivity, as shown in the SEM images in Fig. 3. To ensure that the coating was successful, FTIR and Raman analyses were conducted, and the results confirmed the presence of CMF and collagen (Figs. 4a and 4b).

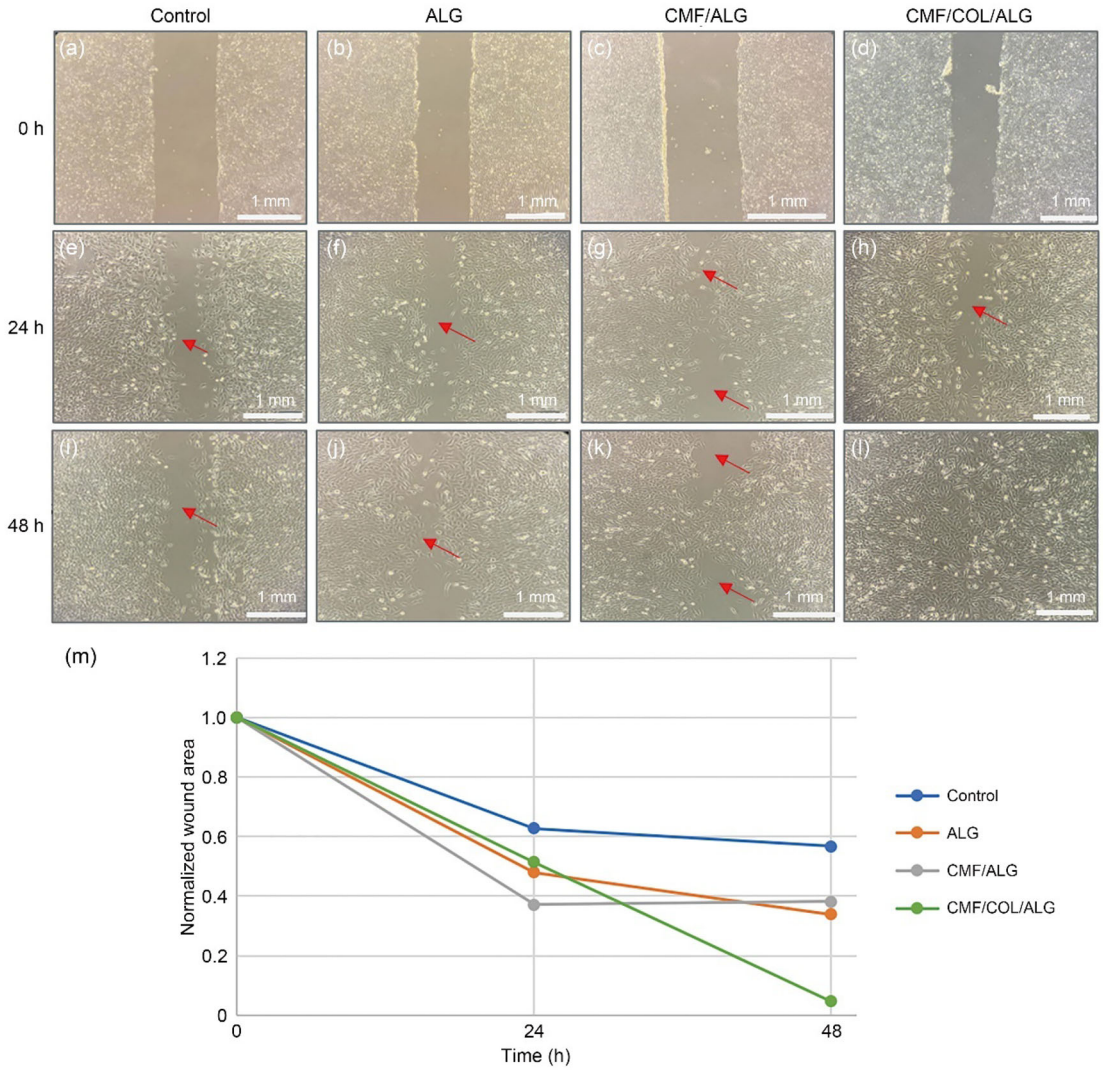

Fig. 9 Scratch test used to evaluate in vitro wound healing. **a**, **e**, **i** Control group. **b**, **f**, **j** Treated with the alginate extract. **c**, **g**, **k** Treated with the CMF/ALG extract. **d**, **h**, **i** Treated with the CMF/COL/ALG extract showing the fastest migration of fibroblasts. **m** Scatter plot showing quantified wound closure area with time. CMF: cellulose microfiber; COL: collagen; ALG: alginate

To act as a proper wound filler, the TWF must have good printability and rheological properties. Different CMF/COL/ALG inks were prepared and tested. As shown in Figs. 5a–5c, 75CMF/COL/ALG (with the highest concentration) had a higher viscosity and therefore improved printability, whereas 25CMF/COL/ALG (with the lowest concentration) was almost like a liquid and completely covered the pores. This is because the viscosity of the ink increases with the CMF concentration owing to its enhanced mechanical properties. This can also be observed in the rheological analysis of the inks shown in Fig. 5d. All inks had a higher storage modulus than loss modulus, indicating that the ink behaves more like a gel than a solution. In addition, the magnitude of the modulus increases with increasing CMF concentration. Viscosity and modulus affect not only printability but also post-printing cell viability owing to high shear stress [35]. Hence, the 75CMF/COL/ALG ink was not selected owing to the remarkably high storage modulus, whereas the 25CMF/COL/ALG ink failed in the printability test. Further optimizations of the inks and printing parameters are possible but because we aimed to address the challenges in treating tunneling wounds, we selected the 50CMF/COL/ALG ink for further experiments.

The designed ink needs to exhibit appropriate and tunable swelling and degradation rates to enhance drug delivery. The presence of hydrophilic groups in the CMFs contributes to the high SR, shown in Fig. 5e [33]. Good swelling properties provide an appropriate 3D structure and favorable environment for cell infiltration, nutrient diffusion, cell migration, and the removal of waste products [31]. Moreover, the relatively high fluid uptake capability of these hydrogels might be an advantage for wound dressing and tissue engineering applications

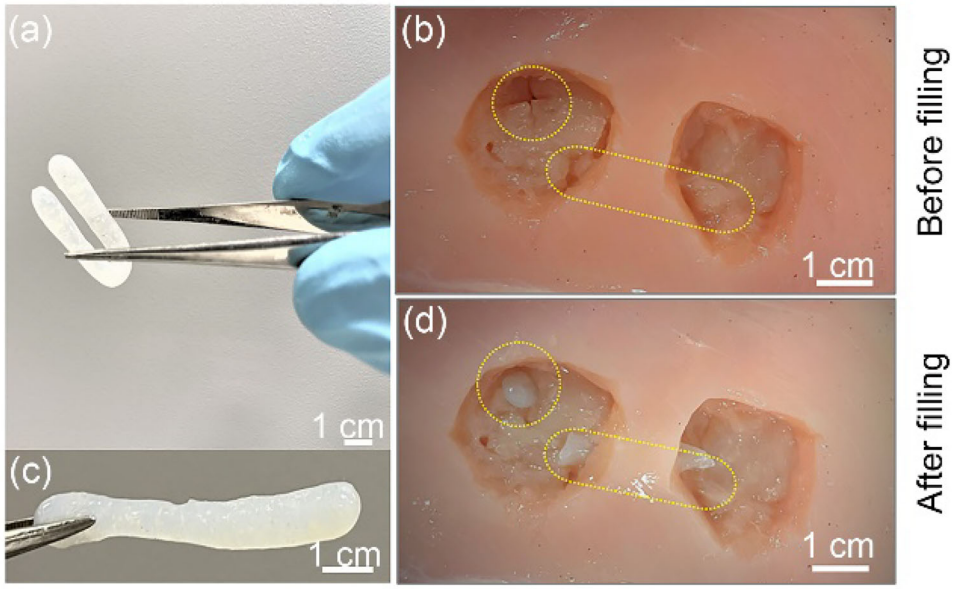

Fig. 10 Chicken tissue model to test the suitability of TWFs in tunneling wound management. **a**, **b** 3D-printed 50CMF/COL/ALG-based TWFs. **c** Wound model with a diameter of 5 mm and a length of 1.5 cm (before packing with TWFs). **d** Packing of tunnel wounds with 3D-printed TWFs (after packing with TWFs). TWFs: tunnel wound fillers; COL: collagen; ALG: alginate

as the TWF can be inserted in a shrunken state and expand to fit a broad range of wound depths and shapes while maintaining the smoothness and softness of the external collagen layer [36]. Furthermore, the weight degradation curve presented in Fig. 5f shows controlled degradation over time, mainly owing to the release of collagen and the breakage of crosslinked polymer chains. Although the weight decreased, the structural stability of the constructs was preserved to some extent, so that they did not completely disintegrate and maintained their cord-like tubular form. The DR is inversely proportional to the CMF concentration; as the CMF concentration increases, the DR decreases. TWF constructs with higher CMF contents underwent lower weight loss owing to the higher crystallinity of cellulose materials undergoing degradation in specific enzymatic, autocatalytic, and hydrolytic conditions [33]. By tuning the concentrations of CMFs, the degradation and in turn, the drug release rate (when loaded with drugs) can be controlled, opening the possibility of controlled drug release [37].

The potential of drug-loaded TWFs for wound healing was evaluated with Baneocin. Baneocin is a common drug used for treating skin wounds. The use of nanocellulose and its high binding capacity due to its surface-area-to-volume ratio allows for tunability and control necessary for advanced drug delivery systems [38]. To evaluate drug release, Baneocin was coated on the TWFs, and the release profile was measured at different pHs, as shown in Fig. 7. Generally, the release stages can be divided into three phases, namely the burst release phase, the nonlinear monotonic release phase, and the final release phase [39]. Both profiles show increasing release with time as expected. However, the burst release is the most prominent phase under acidic conditions (pH 5), which stabilizes after 2 h and maintains a linear phase, with a significantly higher drug release than that under neutral conditions. This is expected as the active ingredient of Baneocin is Neomycin, which is an antibiotic agent that operates better in acidic microenvironments to inhibit bacterial growth and promote healing [40]. These results suggest that 3D-printed TWFs are suitable for sustained drug delivery applications in tunneling wound care treatments.

Upon proving the drug-loading ability of TWFs, the main challenge is the successful incorporation and survival of cells. hMSCs were used in this study as they are multipotent with the ability to differentiate into several lineages, including bone, cartilage, fat, and skin. The staining and AB data in Fig. 8 confirm the cell survival and significant growth over seven days. Furthermore, a scratch test result shown in Fig. 9 corroborates that the CMF/COL/ALG combination provides the best environment for wound healing. These results strongly indicate that the collagen-incorporated CMF/COL/ALG ink might accelerate the wound healing process [41]. Specifically, fish-derived collagen is known to enhance fibroblast and keratinocyte migration within the wound area by activating the genes responsible for wound healing [42] owing to its similarities with human dermal collagen [43].

Finally, the robustness, flexibility, and feasibility of the TWFs were tested using a chicken tissue model (Fig. 10). The 3D-printed CMF/COL/ALG-based TWFs easily penetrated and completely packed the tunnel wound. The softness of the TWFs allows for smooth contact with the surrounding damaged tissue in deep tunnel wounds and provides favorable conditions for healing [44], verifying that the bio-ink (cellulose–collagen blend) developed in this work provides a favorable 3D microenvironment for cell adhesion, migration, and proliferation. These results indicate that cell-laden

TWFs can be bioprinted with the potential to treat tertiary tunneling wounds, where stem cells can be used to augment the healing process or in the regeneration of damaged tissues.

Future studies are required to further optimize the bio-ink composition and fine-tune it with more complex shapes and different drug combinations with diverse release rates, which can help create patient-specific healing methods for chronic wounds, along with possible differentiation of stem cells and in vivo studies before clinical translation.

Conclusions

3D-printed tri-layered drug-eluting TWFs were fabricated as a proof of concept for the treatment of deep tunneling wounds. The extraction of cellulose microfibers from banana stems and coating them with fish skin-derived collagen yielded a good blend that mimics the dermal extracellular matrix and provides balanced mechanical and biological activity. Successful collagen coating was confirmed using SEM, Raman, and FTIR characterization methods. Three different concentrations of CMFs (25, 50, and 75 mg) were tested; the one with lowest CMF concentration had the least viscosity and poor printability, whereas that with the highest concentration was too viscous. Hence, 50CMF/COL/ALG was chosen, and TWFs were bioprinted. The AB data showed that the bioprinting of hMSC-laden TWFs supported cell survival, growth, and proliferation over seven days. The scratch test showed a clear advantage of the CMF/COL/ALG combination, which yielded the best coverage of the wound area. Drug-eluting TWFs incorporating Baneocin showed a controlled drug release rate and opened the possibility for fabricating TWFs with various drugs for wound healing and tunable release rates depending on the healing progression. The structural stability and flexibility of the 3D-printed 50CMF/COL/ALG TWFs indicated that they are suitable for insertion into deep tunneling wounds with twists and turns, as confirmed by the chicken wound model.

Supplementary Information The online version contains supplementary material available at https://doi.org/10.1007/s42242-024-00305-2.

Acknowledgements SV was supported by the start-up funds from New York University Abu Dhabi. This research was partially carried out using the Core Technology Platforms resources at New York University Abu Dhabi. The authors acknowledge the contribution of Dr. Gopinathan Janarthanan in making the graphic abstract for this manuscript.

Author contributions MG contributed to conceptualization, methodology, validation, formal analysis, investigation, visualization, and writing—original draft. NAH contributed to methodology, validation, and formal analysis. SSS contributed to methodology. JRZ contributed to methodology. SA contributed to methodology. SV contributed to conceptualization, fund acquisition, project administration, writing—review and editing, and supervision. All the authors read and approved the manuscript.

Data availability All data generated or analyzed during this study are included in this published article.

Declarations

Conflict of interest The authors declare that they have no conflict of interest.

Ethical approval This article does not contain any studies with human or animal subjects performed by any of the authors.

References

1. Zaid NAM, Sekar M, Bonam SR et al (2022) Promising natural products in new drug design, development, and therapy for skin disorders: an overview of scientific evidence and understanding their mechanism of action. Drug Des Dev Ther 16:23–66. https://doi.org/10.2147/DDDT.S326332
2. Muthusamy S, Kannan S, Lee M et al (2021) 3D bioprinting and microscale organization of vascularized tissue constructs using collagen-based bioink. Biotechnol Bioeng 118(8):3150–3163. https://doi.org/10.1002/bit.27838
3. Rosenbaum AJ, Banerjee S, Rezak KM et al (2018) Advances in wound management. J Am Acad Orthop Sur 26(23):833–843. https://doi.org/10.5435/JAAOS-D-17-00024
4. Sood A, Granick MS, Tomaselli NL (2014) Wound dressings and comparative effectiveness data. Adv Wound Care 3(8):511–529. https://doi.org/10.1089/wound.2012.0401
5. Kim YH, Shim HS, Lee J et al (2022) A prospective randomized controlled multicenter clinical trial comparing paste-type acellular dermal matrix to standard care for the treatment of chronic wounds. J Clin Med 11(8):2203. https://doi.org/10.3390/jcm11082203
6. Kirsner RS, Bohn G, Driver VR et al (2015) Human acellular dermal wound matrix: evidence and experience. Int Wound J 12(6):646–654. https://doi.org/10.1111/iwj.12185
7. Yim H, Cho YS, Seo CH et al (2010) The use of AlloDerm on major burn patients: AlloDerm prevents post-burn joint contracture. Burns 36(3):322–328. https://doi.org/10.1016/j.burns.2009.10.018
8. Kim SW, Shim HS, Lee J et al (2021) Application of paste-type acellular dermal matrix in hard-to-heal wounds. J Wound Care 30(5):414–418. https://doi.org/10.12968/jowc.2021.30.5.414
9. Lee M, Jun D, Choi H et al (2019) Clinical efficacy of acellular dermal matrix paste in treating diabetic foot ulcers. Wounds Compend Clin Res Pract 32(1):50–56
10. Nazari H, Soltani ZE, Asbagh RA et al (2022) Advancing standard techniques for treatment of perianal fistula; when tissue engineering meets seton. Health Sci Rev 3:100026. https://doi.org/10.1016/j.hsr.2022.100026
11. Beaman HT, Howes B, Ganesh P et al (2022) Shape memory polymer hydrogels with cell-responsive degradation mechanisms for Crohn's fistula closure. J Biomed Mater Res Part A 110(7):1329–1340. https://doi.org/10.1002/jbm.a.37376
12. Gao DQ, Glahn JZ, Hsia HC (2023) Engineering a microfibrous composite hydrogel with cell actuation-mediated contractile properties. J Appl Polym Sci 140(48):e54736. https://doi.org/10.1002/app.54736
13. Ghandforoushan P, Golafshan N, Babu Kadumudi F et al (2022) Injectable and adhesive hydrogels for dealing with wounds. Expert Opin Biol Ther 22(4):519–533. https://doi.org/10.1080/14712598.2022.2008353
14. Nike DU, Katas H, Mohd NF et al (2021) Characterisation of rapid in situ forming gelipin hydrogel for future use in irregular deep

cutaneous wound healing. Polymers 13(18):3152. https://doi.org/10.3390/polym13183152
15. Gao Y, Ma QM (2022) Bacterial infection microenvironment-responsive porous microspheres by microfluidics for promoting anti-infective therapy. Smart Med 1(1):e20220012. https://doi.org/10.1002/SMMD.20220012
16. Chen K, Sivaraj D, Davitt MF et al (2022) Pullulan-collagen hydrogel wound dressing promotes dermal remodelling and wound healing compared to commercially available collagen dressings. Wound Repair Regener 30(3):397–408. https://doi.org/10.1111/wrr.13012
17. Singh O, Gupta SS, Soni M et al (2011) Collagen dressing versus conventional dressings in burn and chronic wounds: a retrospective study. J Cutan Aesthetic Surg 4(1):12–16. https://doi.org/10.4103/0974-2077.79180
18. Sundar G, Joseph J, Prabhakumari C et al (2021) Natural collagen bioscaffolds for skin tissue engineering strategies in burns: a critical review. Int J Polym Mater 70(9):593–604. https://doi.org/10.1080/00914037.2020.1740991
19. Liu SQ, Lau CS, Liang K et al (2022) Marine collagen scaffolds in tissue engineering. Curr Opin Biotechnol 74:92–103. https://doi.org/10.1016/j.copbio.2021.10.011
20. Chang GZ, Dang QF, Liu CS et al (2022) Carboxymethyl chitosan and carboxymethyl cellulose based self-healing hydrogel for accelerating diabetic wound healing. Carbohydrate Polym 292:119687. https://doi.org/10.1016/j.carbpol.2022.119687
21. Ohta S, Mitsuhashi K, Chandel AKS et al (2022) Silver-loaded carboxymethyl cellulose nonwoven sheet with controlled counterions for infected wound healing. Carbohydr Polym 286:119289. https://doi.org/10.1016/j.carbpol.2022.119289
22. Diaz-Gomez L, Gonzalez-Prada I, Millan R et al (2022) 3D printed carboxymethyl cellulose scaffolds for autologous growth factors delivery in wound healing. Carbohyd Polym 278:118924. https://doi.org/10.1016/j.carbpol.2021.118924
23. Akatwijuka O, Gepreel MAH, Abdel-Mawgood A et al (2022) Overview of banana cellulosic fibers: agro-biomass potential, fiber extraction, properties, and sustainable applications. Biomass Conv Bioref 14:7449–7465. https://doi.org/10.1007/s13399-022-02819-0
24. Govindharaj M, Roopavath UK, Rath SN (2019) Valorization of discarded marine Eel fish skin for collagen extraction as a 3D printable blue biomaterial for tissue engineering. J Clean Prod 230:412–419. https://doi.org/10.1016/j.jclepro.2019.05.082
25. Michnik A, Kiełboń A, Duch K et al (2022) Comparison of human blood serum DSC profiles in aqueous and PBS buffer solutions. J Therm Anal Calorim 147(12):6739–6743. https://doi.org/10.1007/s10973-021-11008-6
26. Govindharaj M, Hashimi NA, Soman SS et al (2022) 3D bioprinting of human mesenchymal stem cells in a novel tunic decellularized ECM bioink for cartilage tissue engineering. Materialia 23:101457. https://doi.org/10.1016/j.mtla.2022.101457
27. Bolla SR, Mohammed Al-Subaie A, Yousuf Al-Jindan R et al (2019) In vitro wound healing potency of methanolic leaf extract of *Aristolochia saccata* is possibly mediated by its stimulatory effect on collagen-1 expression. Heliyon 5(5):e01648. https://doi.org/10.1016/j.heliyon.2019.e01648
28. Liu CY, Goto D, Hongo C et al (2018) Collagen/cellulose nanofiber blend scaffolds prepared at various pH conditions. ACS Appl Bio Mater 1(5):1362–1368. https://doi.org/10.1021/acsabm.8b00302
29. Lohrasbi S, Mirzaei E, Karimizade A et al (2020) Collagen/cellulose nanofiber hydrogel scaffold: physical, mechanical and cell biocompatibility properties. Cellulose 27(2):927–940. https://doi.org/10.1007/s10570-019-02841-y
30. Połomska M, Kubisz L, Wolak J et al (2021) Effects of temperature on the FT NIR Raman spectra of fish skin collagen. Appl Sci 11(18):8358. https://doi.org/10.3390/app11188358
31. Govindharaj M, Al Hashemi NS, Soman SS et al (2022) Bioprinting of bioactive tissue scaffolds from ecologically-destructive fouling tunicates. J Clean Prod 330:129923. https://doi.org/10.1016/j.jclepro.2021.129923
32. Yang Q, Ma H, Dai ZW et al (2017) Improved thermal and mechanical properties of bacterial cellulose with the introduction of collagen. Cellulose 24(9):3777–3787. https://doi.org/10.1007/s10570-017-1366-y
33. Baniasadi H, Ajdary R, Trifol J et al (2021) Direct ink writing of aloe vera/cellulose nanofibrils bio-hydrogels. Carbohyd Polym 266:118114. https://doi.org/10.1016/j.carbpol.2021.118114
34. Pourali P, Razavianzadeh N, Khojasteh L et al (2018) Assessment of the cutaneous wound healing efficiency of acidic, neutral and alkaline bacterial cellulose membrane in rat. J Mater Sci Mater Med 29(7):90–98. https://doi.org/10.1007/s10856-018-6099-4
35. Chand R, Muhire BS, Vijayavenkataraman S (2022) Computational fluid dynamics assessment of the effect of bioprinting parameters in extrusion bioprinting. Int J Bioprint 8(2):45–60. https://doi.org/10.18063/ijb.v8i2.545
36. Nazarnezhada S, Abbaszadeh-Goudarzi G, Samadian H et al (2020) Alginate hydrogel containing hydrogen sulfide as the functional wound dressing material: in vitro and in vivo study. Int J Biol Macromol 164:3323–3331. https://doi.org/10.1016/j.ijbiomac.2020.08.233
37. Milojević M, Harih G, Vihar B et al (2021) Hybrid 3D printing of advanced hydrogel-based wound dressings with tailorable properties. Pharmaceutics 13(4):564. https://doi.org/10.3390/pharmaceutics13040564
38. Plappert SF, Liebner FW, Konnerth J et al (2019) Anisotropic nanocellulose gel-membranes for drug delivery: tailoring structure and interface by sequential periodate-chlorite oxidation. Carbohydr Polym 226:115306. https://doi.org/10.1016/j.carbpol.2019.115306
39. Huo PP, Han XX, Zhang WY et al (2021) Electrospun nanofibers of polycaprolactone/collagen as a sustained-release drug delivery system for artemisinin. Pharmaceutics 13(8):1228. https://doi.org/10.3390/pharmaceutics13081228
40. Pastar I, Stojadinovic O, Yin NC et al (2014) Epithelialization in wound healing: a comprehensive review. Adv Wound Care 3(7):445–464. https://doi.org/10.1089/wound.2013.0473
41. Ehrlich HP, Hunt TK (2012) Collagen organization critical role in wound contraction. Adv Wound Care 1(1):3–9. https://doi.org/10.1089/wound.2011.0311
42. Elbialy ZI, Atiba A, Abdelnaby A et al (2020) Collagen extract obtained from Nile tilapia (*Oreochromis niloticus* L.) skin accelerates wound healing in rat model via up regulating VEGF, bFGF, and α-SMA genes expression. BMC Vet Res 16(1):352. https://doi.org/10.1186/s12917-020-02566-2
43. Furtado M, Chen L, Chen ZH et al (2022) Development of fish collagen in tissue regeneration and drug delivery. Eng Regener 3(3):217–231. https://doi.org/10.1016/j.engreg.2022.05.002
44. Li J, Yu F, Chen G et al (2020) Moist-retaining, self-recoverable, bioadhesive, and transparent in situ forming hydrogels to accelerate wound healing. ACS Appl Mater Interfaces 12(2):2023–2038. https://doi.org/10.1021/acsami.9b17180